

Article

Preparation and Characterization of Lauric Acid/Modified Fly Ash/Graphene Composite as Low-Cost and Eco-Friendly Phase Change Materials for Thermal Energy Storage

Peng Liu ^{1,2,3}, Xinglan Cui ⁴, Yajing Wang ^{1,2,3,*}, Zhikai Zhang ⁵, Jun Rao ^{1,2,3}, Shuai Jiang ⁶ and Xiaobin Gu ^{7,*}¹ School of Gems and Materials Technology, Hebei GEO University, Shijiazhuang 050031, China² Hebei Key Laboratory of Green Development of Rock and Mineral Materials of Hebei Province, Shijiazhuang 050031, China³ Engineering Research Center for Silicate Solid Waste Resource Utilization of Hebei Province, Shijiazhuang 050031, China⁴ The National Engineering Research Center for Environment-Friendly Metallurgy in Producing Premium Non-Ferrous Metals, GRINM Resources and Environmental Technology Corporation Limited, Beijing 100088, China⁵ School of Water Resources and Environment, Hebei GEO University, Shijiazhuang 050031, China⁶ Shengli Xinda New Material Company Ltd., Dongying 257000, China⁷ Materials Interfaces Center, Shenzhen Institutes of Advanced Technology, Chinese Academy of Sciences, Shenzhen 518005, China

* Correspondence: wyjbs@hgu.edu.cn (Y.W.); guxb@ms.giec.ac.cn (X.G.)

Abstract: Fly ash is a kind of industrial solid waste that is considered “hazardous waste”. In this study, a supporting matrix of modified fly ash (MFA) was employed to package lauric acid (LA) via a facile direct impregnation method involving less experimental error. A low-cost and eco-friendly form-stable phase change material (PCM) of LA/MFA/graphene (G) was fabricated, with G as the thermal conductivity enhancer. The preparation and leakage testing of an LA/MFA/G form-stable PCM (FSPCM) were investigated in detail. The leakage test results indicated that good package efficiency was obtained using MFA with a higher specific surface area and richer pore structure to pack the LA. Then, LA/MFA/G composites were characterized via scanning electronic microscope (SEM), Fourier transform infrared spectroscopy (FTIR), differential scanning calorimeter (DSC), and thermal gravimetric analyzer (TGA). The results showed that excellent form stability was obtained by adding MFA as the supporting matrix. The SEM analysis indicated that LA could be well dispersed into the structure of MFA. The FTIR analysis demonstrated that the components of the FSPCM were quite compatible. The results of the DSC illustrated that LA/MFA/G (5 wt. %) had a melting point of 45.38 °C and a latent heat of 41.08 J/g. The TGA analysis revealed that the prepared FSPCM had better thermal stability compared with LA within its working temperature range. In addition, the effects of G on the heat transfer performance of the prepared FSPCM were examined. In short, using MFA with a higher specific surface area and richer pore structure to pack the LA via a simple preparation process with less experimental error can contribute to good performance. The research not only improved the comprehensive utilization of solid waste, but also promotes the application of FSPCM in the field of building energy conservation.

Keywords: lauric acid; modified fly ash; graphene; FSPCM; thermal energy storage



Citation: Liu, P.; Cui, X.; Wang, Y.; Zhang, Z.; Rao, J.; Jiang, S.; Gu, X. Preparation and Characterization of Lauric Acid/Modified Fly Ash/Graphene Composite as Low-Cost and Eco-Friendly Phase Change Materials for Thermal Energy Storage. *Energies* **2023**, *16*, 5666. <https://doi.org/10.3390/en16155666>

Academic Editor: Merce Segarra

Received: 28 June 2023

Revised: 8 July 2023

Accepted: 15 July 2023

Published: 28 July 2023



Copyright: © 2023 by the authors. Licensee MDPI, Basel, Switzerland. This article is an open access article distributed under the terms and conditions of the Creative Commons Attribution (CC BY) license (<https://creativecommons.org/licenses/by/4.0/>).

1. Introduction

Energy consumption has increased rapidly due to economic development and rising living standards [1]. As a result, the global energy challenge has become a threat to humanity in this century [2]. In particular, the global consumption of electricity produced by thermal power plants is growing [3]. Simultaneously, the demand for alternative power supplies caused by the global energy crisis is also increasing [4]. However, industrial waste

emissions from electricity and heat generation create challenges for the low-carbon or net-zero carbon economy [5]. Among these, industrial waste fly ash (FA) as a by-product of coal combustion in thermal power plants has become one of the most important dangerous industrial solid wastes. More than 620 million tons of FA was produced in China in 2019; 540 million tons of it was produced by some important industries, such as electric power [6]. Although FA has partly been recycled for porous materials and construction materials such as plaster, brick, wallboard, cement, and concrete [7–9], FA waste is still massive, and more than 3000 million tons of it will destroy the local ecological environment due to potentially toxic trace elements and heavy metal elements, as well as other contaminants [10–12]. In addition, FA occupies a large area of soil; therefore, the disposal of FA is technically difficult. More efforts have been undertaken to improve the comprehensive utilization of FA to develop new approaches and applications.

Simultaneously, much attention has been paid to developing renewable energy sources and improving energy utilization and management around the world, owing to the energy crisis and environmental pollution caused by carbon-based fossil energy sources such as coal [13,14]. Phase change materials (PCMs) are advantageous in thermal energy storage, and are considered to be one of the main technologies to address global energy challenges through improving energy efficiency and achieving energy savings [15,16]. As latent heat energy storage materials, PCMs have the ability to adsorb and release substantial thermal energy during the melting and solidifying process, with a high energy storage density and cost savings [17]. Among the investigated PCMs, fatty acids such as lauric acid (LA) are regarded as one of the most promising PCMs for extensive low-temperature application prospects, due to its low vapor pressure, low cost, ready availability, good chemical compatibility, thermal stability, non-corrosivity, non-toxicity, and excellent thermal properties [18,19]. However, the poor thermal conductivity and leakage problems of fatty acids restrict their practical application [20]. Therefore, much research is required to resolve the two drawbacks. On the one hand, various kinds of thermal conductivity enhancers can be introduced to enhance LA's thermal conductivity, which is considered a simple and effective method [21]. Among the various conductivity enhancers, graphene (G) is a relatively ideal conductivity enhancer that is extensively employed due to its ultrahigh thermal conductivity, high specific surface area, and light weight [22–24]. On the other hand, many efforts have been made to solve the leakage problem of fatty acids. A simple and effective method is to adsorb PCMs into porous minerals to fabricate form-stable PCMs (FSPCMs). The porous minerals that can act as supporting materials are as follows: diatomite (DT) [25,26], sepiolite [27,28], vermiculite [29,30], attapulgite [31,32], and so on. The package efficiencies of these raw porous minerals are acceptable. However, the costly, relatively exiguous, and exhaustive characteristics of raw porous minerals reduce the practical application value of porous minerals-based FSPCMs. Hence, developing high-performance FSPCMs based on low-cost and environmentally friendly supporting materials remains a significant challenge. It is necessary to develop other lightweight porous support materials with large specific surface areas and low costs.

Interestingly, the above-mentioned FA is quite easily available, cheap, and abundant. Moreover, FA comprises abundant and complex anthropogenic materials with different mineral phases [33]. Fortunately, many mineral chemical components in FA are similar to the components in some porous minerals. Based on this fundamental knowledge, FA could theoretically be employed as a supporting matrix to prevent the leakage of fatty acids. Furthermore, the initial feasibility of FA has been confirmed by some scholars to reduce the costs of supporting materials and improve the comprehensive utilization level of FA in the past few years [33–42]. On the one hand, previous research showed that FA can be employed as a support material to pack LA to fabricate FSPCMs, according to the above-mentioned literature. However, the preparation processes and procedures are complex. Moreover, the latent heat of FSPCMs based on directly employing FA as a supporting material was found to be lower compared with conventional supporting materials. Even though the latent heat of FSPCMs based on FA was much lower compared

with conventional supporting materials, a demand for the high-value utilization of FA and its advantage of zero raw material costs still promotes the development of FSFCMs based on FA. Therefore, it is urgent to develop a treatment method to modify FA with large specific surface areas; this is of great significance to this research.

On the other hand, it is worth noting that excellent results to improve PCM loading by employing different treatment methods to modify porous minerals have been achieved. Hence, suitable approaches can be applied to the modification of industrial solid wastes such as FA. Among the different treatment methods, the acid-leaching treatment of FA has been proven to be feasible. With its promise to improve the loading capacity of PCMs, there is further need to evaluate the efficiency of this technology. Therefore, systematic experiments should be proposed and used to explore the package efficiency of modified FA as a supporting material. In this study, we first developed a porous support material with large specific surface areas, light weight, and low cost, in order to improve the package efficiency of FA. Then, LA, modified FA, and G were used as the PCM, supporting matrix, and thermal conductivity enhancer, respectively. A low-cost and eco-friendly FSFCM of LA/MFA/G was prepared via a simple and facile direct impregnation method involving a simple process. Leakage testing was performed, and the physical structure and thermal properties were systemically investigated. The feasibility and performance of using MFA to pack LA via the facile direct impregnation method with reduced operation error were systemically examined. This research into the preparation feasibility and performance evaluation of LA/MFA/G FSFCM could not only broaden the comprehensive utilization field for FA, but also demonstrate potential in fabricating new construction materials for energy savings in buildings. More importantly, the sustainability of FA supporting material is of vital importance for practical applications.

2. Experiments

2.1. Materials

In this study, the LA used in this study (98.5% pure, analytical grade) was supplied by Sinopharm Chemical Reagent Co., Ltd. (Shanghai, China). The FA sample was provided by Shijiazhuang Thermal Power Plant. The chemical composition of FA is listed in Table 1. Sulfuric acid was obtained from Tianjin Damao Chemical Reagent Co., Ltd., China. Before their use, the samples of raw FA were dried at 110 °C for 2 h to remove humidity. The G was used as a thermal conductivity enhancer, and was purchased from Suzhou Tanfeng Technology Co., Ltd., Suzhou, China.

Table 1. Chemical composition of FA before and after modification.

Item	SiO ₂	Al ₂ O ₃	Fe ₂ O ₃	TiO ₂	K ₂ O	Na ₂ O	CaO	MgO	Others
FA	49.120	37.042	4.859	1.555	1.145	0.751	2.734	0.614	2.18
MFA [37]	52.490	37.433	4.032	1.564	1.118	0.784	0.909	0.534	1.136

2.2. Preparation of LA/MFA/G

A schematic diagram of the preparation processes for LA/MFA/G is shown in Figure 1. The whole preparation process can be divided into three steps, i.e., the modification of FA, the synthesis of LA/MFA FSFCM, and the preparation of LA/MFA/G FSFCM. Information for all of the composite samples is shown in Table 2.

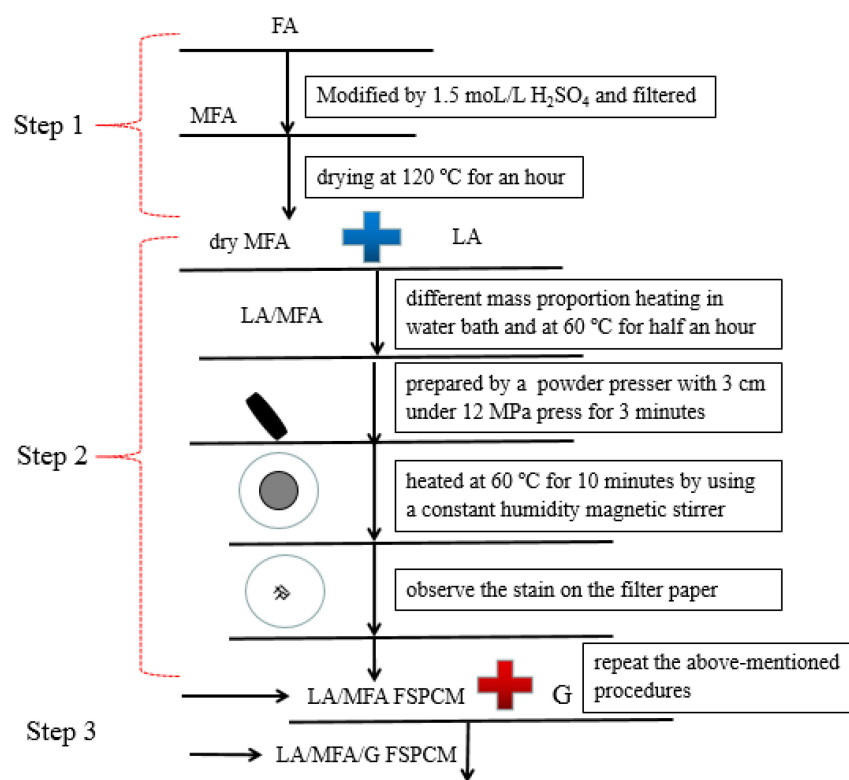


Figure 1. Schematic diagram of preparation process of LA/MFA/G FSPCM.

Table 2. The basic proportions of the LA/MFA and LA/MFA/G composites.

Step	Sample Name	Composition Ratio (wt. %)	Leakage Ratio (%)	Leakage Area (cm ²)	Deformation (Yes/No)	Leakage (Yes/No)
2	S1-1	Pure LA	45.57	122.66	Yes	Yes
2	S1-2	60 LA + 40MFA	19.76	45.34	Yes	Yes
2	S1-3	50 LA + 50MFA	11.37	38.74	Yes	Yes
2	S1-4	40 LA + 60MFA	5.70	29.45	Yes	Yes
2	S1-5	30 LA + 70MFA	1.37	6.83	No	Yes
2	S1-6	20 LA + 80MFA	0	0	No	No
2	S2-1	30 LA + 70MFA/1G	1.23	6.38	No	Yes
2	S2-2	30 LA + 70MFA/3G	0.77	5.62	No	Yes
2	S2-3	30 LA + 70MFA/5G	0.23	1.18	No	Yes
2	S2-4	30 LA + 70MFA/7G	0	0	No	No
3	S3-1	27.5 LA + 72.5MFA/1G	0	0	No	No
3	S3-2	27.5 LA + 72.5MFA/3G	0	0	No	No
3	S3-3	27.5 LA + 72.5MFA/5G	0	0	No	No

2.2.1. Modification of FA

In the first step, the FA was treated using sulfuric acid. The detailed process was as follows. Firstly, a certain amount of FA was added to a 250 mL beaker with 1.5 mol/L sulfuric acid solution. Secondly, the beaker with the mixture of FA and sulfuric acid solution was placed on a magnetic stirrer and stirred for half a day at 50 rpm. After that, the obtained product was filtered with a medium-speed filter. Then, the sediment was repeatedly washed until it was neutral. During the rinse, sediment was repeatedly filtered using a vacuum filter. Finally, the sediment was dried in a drying oven for 12 h at 110 °C. After this, the modified FA was obtained. The modification process of FA also refers to our previous description, and the X-ray fluorescence results (XRF) of the MFA are provided in Table 1.

2.2.2. Synthesis of LA/MFA FSPCM

In the second step, the LA/MFA composite was synthesized via a simple and facile direct impregnation method. The fabricating procedures were as follows. The MFA was dried at 120 °C for 60 min before use. Then, a certain amount of LA and MFA were weighed and uniformly mixed by hand in a 250 mL beaker using a glass rod according to different mass ratios of 6:4, 5:5, 4:6, 3:7, and 2:8. Then, the beakers with the corresponding mixture of different mass ratios were heated to 60 °C in a water bath, and continuously stirred for half an hour. After the LA was completely melted, all of the beakers were cooled to room temperature. Thus, the LA/MFA composites were fabricated. After that, the synthesized composites were pressed into tablets with the same quality, shape, and size according to the literature [35,43]. Finally, the leakage tests of the tablet samples were carried out to examine the leakage performance of LA/MFA composites at a heating temperature of 60 °C for 10 min, according to experiments in literature [35,43]. The leakage test results are shown in Table 2. All of the composite samples are also described in Table 2.

2.2.3. Preparation of LA/MFA/G FSPCM

In the third step, on the basis of experiment exploration, the determined dried LA and MFA were weighed to specified amounts according to different mass fractions of 6:4, 5:5, 4:6, 3:7, and 2:8, and fully mixed in 250 mL beakers. Then, G with a certain weight percentages of 1 wt. %, 3 wt. %, 5 wt. %, and 7 wt. % was added into the beakers with LA/MFA FSPCM and evenly mixed on a magnetic stirrer. Subsequently, beakers with their corresponding mixtures were placed in a 60 °C water bath for 30 min to fabricate the LA/MFA/G composites. During the fabrication process, the mixture was continuously stirred using a glass rod. After the LA was fully adsorbed into the MFA, the synthesized mixture was cooled down to room temperature. The LA/MFA/G composites were obtained following the above-mentioned procedures. Then, the leakage tests of the LA/MFA/G composites were performed in line with the method mentioned above. The leakage testing results determined the package efficiency and formability of the prepared LA/MFA/G composites. In this way, the LA/MFA/G FSPCM was obtained.

2.3. Characterization

A scanning electron microscope (SEM, PhenomProX) was used to study the microstructural morphologies of the LA, MFA, G, LA/MFA FSPCM, and LA/MFA/G FSPCM. A Fourier transform infrared spectrometer (FTIR, Thermo Scientific, USA) was employed to record the chemical compatibility among the components of the LA/MFA/G FSPCM. The wavenumber was changed from 400 to 4000 cm^{-1} with a resolution of 2 cm^{-1} using KBr pellets. Thermogravimetric analysis (TGA, Q600) was utilized to investigate the stability of the fabricated FSPCMs. The operating temperature ranged from 25 °C to 400 °C, with a heating rate of 20 °C/min under an N_2 atmosphere. A differential scanning calorimeter (DSC, Q100) was used to determine the thermal properties of the FSPCMs with a heating rate of 10 °C/min in an N_2 atmosphere, and its mean deviation of latent heat accuracy and phase change temperature were 0.1% and 0.1 °C, respectively. XRF (PANalytical Axios) was used to determine the oxide content. To investigate the thermal energy storage/release performance of the samples and examine the effect of G on the heat transfer efficiency, heat storage/release curves of the prepared FSPCMs were measured using an intelligent paperless recorder. The operating temperature ranged from 20 °C to 80 °C and 80 °C to 20 °C, for the heating process and the freezing process, respectively. In addition, the leakage results of liquid LA were evaluated in terms of the leakage area and the leakage ratio in the second step. The results are listed in Table 2. In this study, the leakage ratio was the leakage mass of LA divided by the total mass of LA in the corresponding composite [44].

3. Results and Discussion

3.1. Leakage Test Results of the Prepared FSPCMs

3.1.1. Leakage Test Results of LA/MFA Composites

The leakage test results of the synthesized LA/MFA composites were obtained after heating at 60 °C, and were also reported in our previous research [43]. The stain of the liquid LA in the composite on the filter decreased with the mass ratio of LA to MFA, decreasing from 6:4, 5:5, and 4:6 to 3:7. According to our previous study, when the ratio of LA to MFA was 2:8, the LA /MFA composite did not leak [42]. The leakage of the composites became increasingly worse with the increasing LA mass fraction. In other words, increasing the mass fraction of FA prevented leakage of the samples. Moreover, the shape stability of the composites was consistent with the leakage stain results of LA in the composites. Thus, the prepared LA/MFA composite with a mass ratio of LA to MFA at 3:7 was initially considered to be form-stable without LA leakage.

In short, MFA can successfully confine LA and restrict the leakage of LA. Moreover, these results revealed that LA/MFA composites had better form stability than LA/FA composites. In other words, the modification of FA could improve the loading capacity and package efficiency of raw FA [42].

3.1.2. Leakage Test Results of LA/MFA/G Composites

Based on the exploratory experiment mentioned above, the loading capacity of LA in MFA was determined as 3:7. Considering the high storage capacity and package efficiency, G weight percentages of 1 wt. %, 3 wt. %, 5 wt. % and 7 wt. % were introduced into the composite with an LA to MFA mass ratio of 3:7. The leakage results are displayed in Figure 2. Different stains were observed on the filter papers of the corresponding samples. As seen from Figure 2a, even though the S2-1, S2-2, and S2-3 samples showed no deformation, there were leakage stains of LA on the filter papers of the S2-1, S2-2, and S2-3 composites in Figure 2b. In particular, obvious leakage of LA in the S2-1 sample was observed. When the mass ratio of LA to MFA was 3:7 with 7 wt. % G, no deformation and stain were observed on the filter paper in Figure 2a,b. Namely, no leakage occurred on the filter paper after heating LA/MFA/G with an LA to MFA mass ratio of 3:7 and 7 wt. % G. In addition, it also demonstrated that G contributed to the adsorption capacity of LA, and restricted the leakage of liquid LA. In other words, G also had an important effect on the loading capacity and package efficiency of MFA, in addition to its ability to improve thermal conductivity.

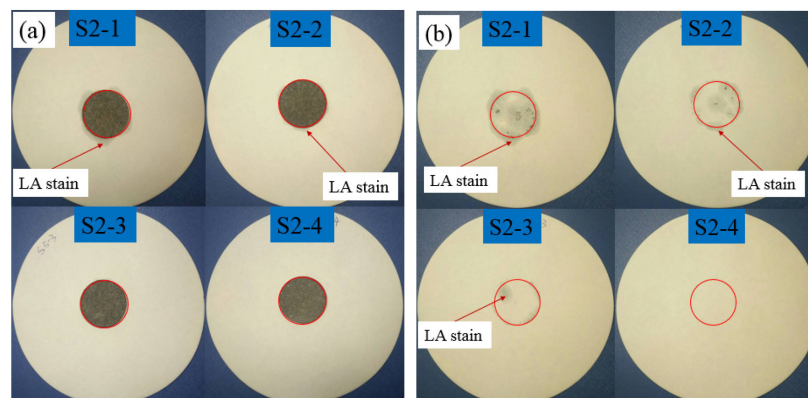


Figure 2. Deformations of LA/MFA/G samples after heating at 60 °C. (a) Liquid leakage of samples after heating (b) liquid stain on the filter paper after heating.

These findings were good for predicting the leakage extent of the fabricated composites to investigate the relationships between the G mass fraction and leakage of the LA/MFA/G composites. The relationships in the second step between the leakage results and different mass fractions of G are shown in Figure 3, according to Table 2. As seen from Figure 3a,

when the synthesized composites were heated for 10 min, there were good negative correlations between the leakage ratio and mass fraction of G added in the composites. Similar relationships were also found between the leakage area and the mass fraction of G, as shown in Figure 3b. These results help to evaluate the leakage of LA/MFA/G composites. The above-mentioned relationships were described as follows:

$$Y_1 = -0.2117X_1 + 1.4050, R^2 = 0.9667$$

where Y_1 refers to the leakage ratio of the LA/MFA/G composite, in cm^{-2} . X_1 refers to the mass fraction of G added, in %.

$$Y_2 = -1.1784X_2 + 8.0064, R^2 = 0.8783$$

where Y_2 refers to the leakage area of the LA/MFA/G composite, in cm^{-2} . X_2 refers to the mass fraction of G added, in %.

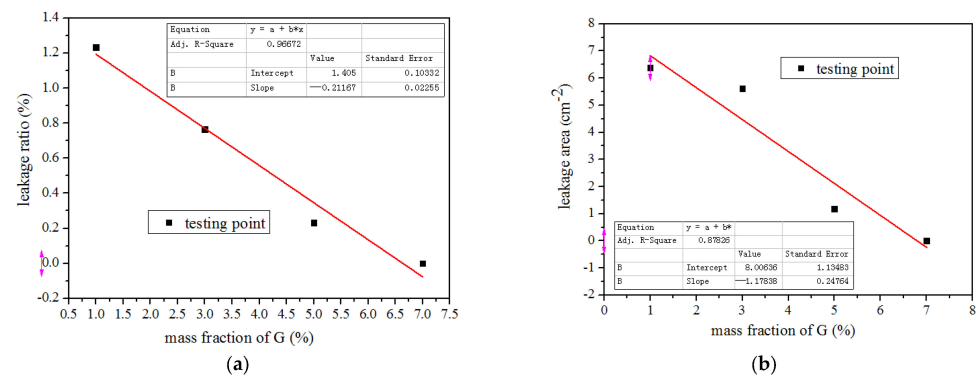


Figure 3. Relationships between the leakage results and different mass fractions of G. (a) Relationships between leakage ratio and mass fractions of G (b) Relationships between leakage area and mass fractions of G.

Considering the relatively high cost of G, when the optimized mass ratio of LA to MFA was 27.5:72.5, G weight percentages of 1 wt. %, 3 wt. %, and 5 wt. % were added into the LA/MFA composites. The leakage test results are provided in Figure 4; when the mass ratio of LA to MFA was 27.5:72.5 with 1 wt. % G, little leakage staining occurred in the S3-1 sample on the filter paper in Figure 4b, while no leakage stains of the S3-2 and S3-3 samples can be observed in Figure 4b. This means that the leakage of LA in LA (27.5 wt. %)/MFA (72.5 wt. %)/G (1 wt. %) did not appear. Finally, the preferred mass ratio of LA to MFA was determined to be 27.5:72.5.

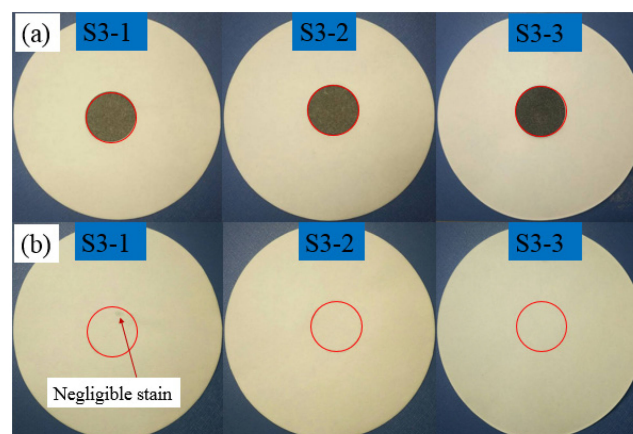


Figure 4. Liquid stains of LA in optimization of LA/MFA/G on the filter paper obtained at 60 °C. (a) Liquid leakage of samples after heating (b) liquid stain on the filter paper after heating.

3.2. Microstructure of the Prepared Composites

Figure 5 shows the SEM images of FA, MFA, G, and LA/MFA/G FSPCM. Figure 5a shows that raw FA exhibited spherical structures with different diameters and tiny hairy surfaces, like balls [35]. The MFA in Figure 5b consists of the different pore structures on the sphere surface, which are beneficial to absorb liquid LA, together with numerous hairy structures on the spherical surface, manifesting the modification that enables FA to act as a supporting matrix. In Figure 5c, the G is described as sheet structures with a stepped layered appearance. As indicated in Figure 5d–f, the hairiest structures of MFA and the porous structure of G disappeared because the melted LA was impregnated into the pore structure of the MFA fragment, absorbed onto the hairy surface microsphere structure of MFA, and dispersed onto the sheet structure surface of G. This demonstrated that liquid LA could be loaded and packaged by an MFA supporting matrix. That is to say, MFA can restrict the leakage of liquid LA. Moreover, the melted LA was covered on the surface of the sheet structure of G, indicating that G can not only successfully mix with MFA, but can also construct new heat transfer channels among the LA molecules.

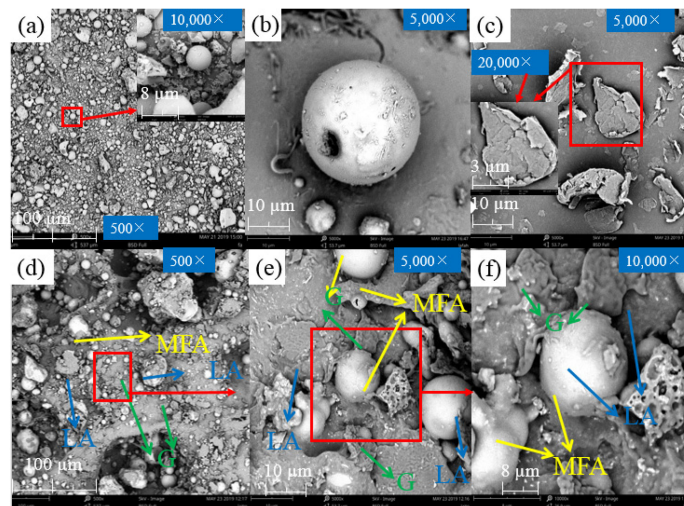


Figure 5. SEM images of (a) FA, (b) MFA, (c) G, and (d–f) LA/MFA/G.

3.3. Chemical Compatibility of the Prepared Composites

The LA, FA, MFA, LA/MFA composite, G, and LA/MFA/G FSPCM were examined via FTIR spectroscopy. Figure 6 shows the FTIR spectra of the selected samples. For LA, the characteristic peaks at 723 cm^{-1} and 937 cm^{-1} were associated with in-plane swinging vibrations and the out-of-plane bending vibrations of O-H, respectively. Meanwhile, the characteristic peaks at 1704 cm^{-1} , 937 cm^{-1} , and 937 cm^{-1} signified the stretching vibrations of the C=O group, and the C-H bond in the $-\text{CH}_2$ and $-\text{CH}_3$ groups, respectively [45,46]. For the MFA, the O-S-O stretching vibration, Si-O-Si stretching vibration, and Si-O-Al asymmetric vibration were observed at 551 , 927 , and 1094 cm^{-1} , respectively [40]. For the G, no strong peak was observed corresponding to the research, indicating the comparatively pure structure of the sheets [47,48]. In the FTIR spectrum of the LA/MFA composite, the main characteristic peaks of the LA could readily be observed. This suggests that there was only physical interaction between the LA and MFA. Similarly, in the FTIR spectrum of LA/MFA/G FSPCM, the main characteristic peaks of the LA were also obvious. This suggests that there were physical interactions only among the LA, MFA, and G. The main characteristic peaks of the LA emerged in the LA/MFA composite and LA/MFA/G FSPCM, indicating that no chemical reactions occurred among LA, MFA, and G in the preparation process. The FTIR results demonstrated that MFA and G had excellent chemical compatibility with LA, indicating that LA/MFA/G FSPCM is suitable as a thermal storage material.

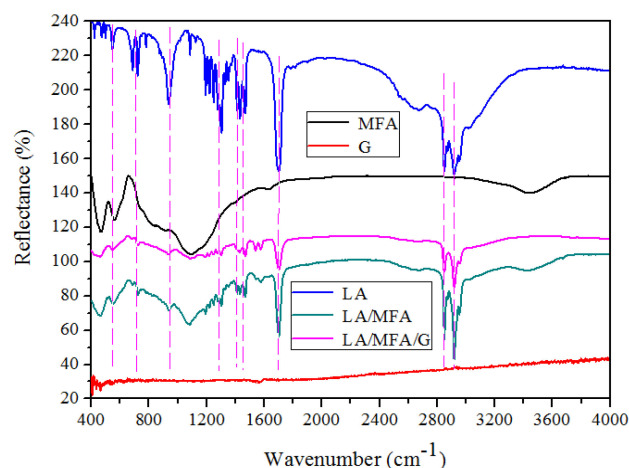


Figure 6. FTIR spectra of LA, MFA, G, LA/MFA, and LA/MFA/G.

3.4. Thermal Properties of the Prepared FSPCMs

Figure 7 shows the DSC curves of LA, LA/raw FA FSPCM, LA/MFA FSPCM, and LA/MFA/G FSPCM. The phase change temperature and the latent heat data are presented in Table 3. As shown in Figure 7 and Table 3, the melting and freezing temperatures were determined to be 44.26 °C and 41.23 °C for LA, respectively; in contrast, they were determined to be 45.74 °C and 41.39 °C for LA/raw FA FSPCM, 45.39 °C and 40.82 °C for LA/MFA FSPCM, and 45.58 °C and 40.22 °C for LA/RFA/G (5 wt. %) FSPCM. The latent heats of melting and freezing were measured as 179.9 J/g and 177.6 J/g for LA, 44.93 J/g and 43.60 J/g for LA/raw FA FSPCM, 49.71 J/g and 47.86 J/g for LA/MFA FSPCM, and 41.08 J/g and 39.32 J/g for LA/MFA/G (5 wt. %) FSPCM, respectively.

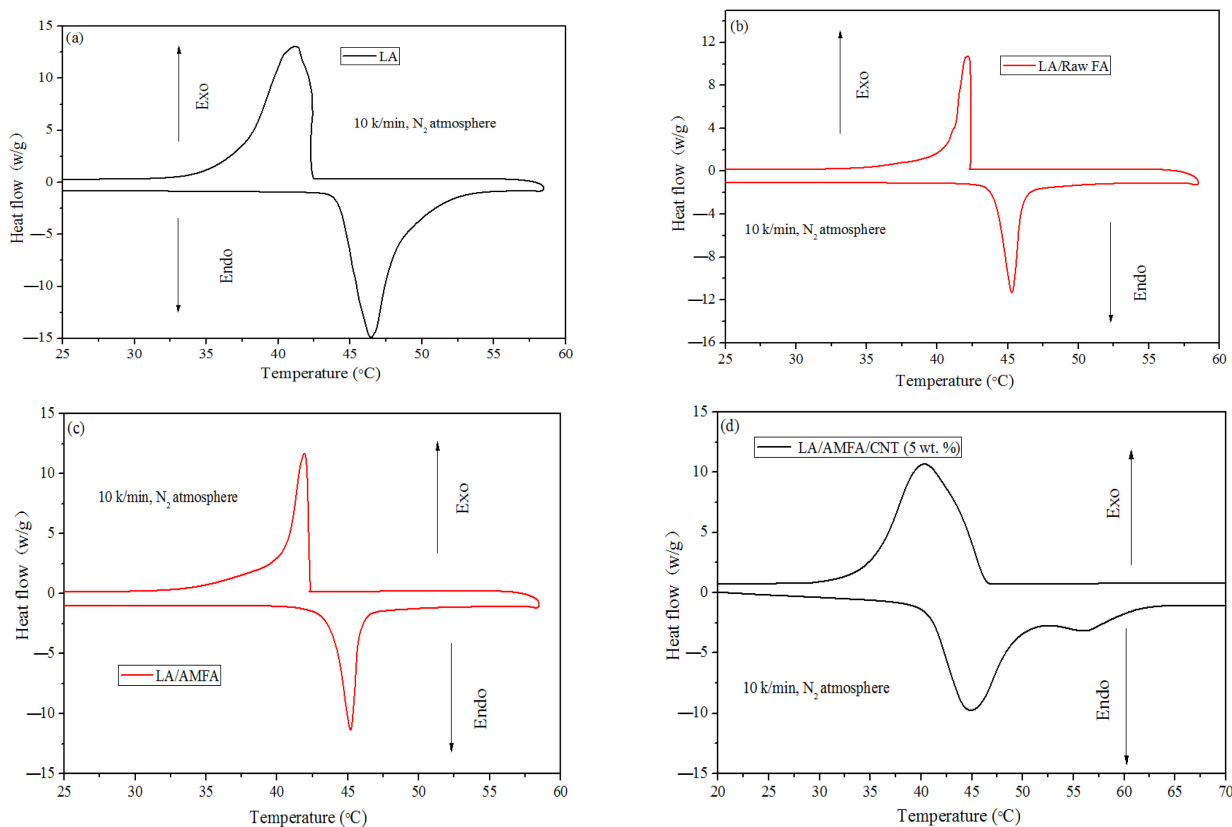


Figure 7. DSC curves of LA and LA/raw FA, LA/MFA, and LA/MFA/G (5 wt %). (a) DSC curve of LA (b) DSC curve of LA/raw FA (c) DSC curve of LA/MFA (d) DSC curve of LA/MFA/G (5 wt %).

Table 3. Thermal properties of the selected samples.

Samples	Loading Rate of LA (%)	Melting Temperature (°C)	Solidifying Temperature (°C)	Measured Latent Heat of Melting (J/g)	Measured Latent Heat of Solidification (J/g)	Calculated Loading Rate of LA (%)
LA	100	44.29	41.23	179.6	177.9	100
LA/raw FA (leakage)	25%	45.74	41.39	44.93	43.60	24.04
LA/MFA	30	45.39	40.82	49.71	47.86	27.22
LA/MFA/G (5 wt. %)	27.5	45.38	40.22	41.08	39.26	22.87

Compared with the pure LA, the phase change temperature of the LA/RFA/G FSPCM changed slightly (approximately 1.09 °C for melting and 1.01 °C for freezing), indicating that using raw FA or MFA as a supporting material for LA had no influence on the phase change temperature. The decrease in latent heat of the prepared FSPCMs was due to the fact that raw FA and MFA had no phase change latent heat. However, owing to the introduction of G, and particularly to the loading capacity enhanced by the fragment mixture of MFA, the MFA and G could adsorb the LA better and more extensively, thereby preventing leakage and presenting a high latent heat. As a result, the LA largely infiltrated into the pores of MFA, and the phase change property was higher than that of LA/raw FA. This is consistent with the results of the previous packaging leakage experiments. Furthermore, it was mainly due to the relative high packaging efficiency compared to the MFA. Simultaneously, this indirectly confirms the validity of the SEM images and FTIR spectra from another perspective.

The loading fractions of the supporting matrix for each kind of FSPCM were obtained with the following Equation [49,50]:

$$M = \Delta H_{\text{FSPCM}} / \Delta H_{\text{LA}} \times 100\%$$

where μ is the corresponding loading fraction of LA in FSPCM, in %; and ΔH_{FSPCM} and ΔH_{LA} are the latent heats of FSPCM and LA, J/g, respectively. The calculated values and theoretical estimations are shown in Table 3. As can be seen from Table 3, the calculated adsorptive capacities of LA were retained at 27.22% and 22.87% in the LA/MFA and LA/MFA/G (5 wt. %) FSPCM, respectively, which were both slightly lower than the loading rates of LA in the LA/MFA and LA/MFA/G composites without leakage. On the whole, they were basically consistent with the results of the previous leakage test of composites shown in Figure 2b.

Based on further analysis, the calculated latent heat capacities of LA/MFA/G seepage-free FSPCM were also lower than the theoretical values, which were consistent with the mass fractions of LA. The reason may be that extremely weak physicochemical effects occurred among small fractions of the LA, MFA, and G. The confinement of LA by MFA and G probably hindered the crystal arrangements and orientation of the LA molecule chains.

Table 4 lists a comparison of the thermal properties between the synthesized FSPCMs and some form-stable composite PCMs from results in some of the literature. From Table 4, it can be seen that the latent heat of LA/MFA/G (5 wt. %) FSPCM (41.08 J/g for the melting process) was much higher than those of some form-stable composite PCMs that were prepared for thermal energy storage in low temperature fields under 100 °C. It can be seen that the MFA used as support material has a much better package efficiency than that of active aluminum oxide, gypsum, TiO₂-FA, vermiculite, and RFA. Correspondingly, the latent heat of the fabricated LA/MFA/G (5 wt. %) FSPCM in this study is higher than those of the above-mentioned support materials. Moreover, even though the 27.5 wt. % package efficiency of MFA was lower than that of the high-cost CNT which obtained a 44.8 wt. % package efficiency, the latent heat of the fabricated LA/MFA/G (5 wt. %) FSPCM in this study was more or less with the latent heat of LA (44.8 wt. %)/CNT. Therefore, the

fabricated FSPCMs in this study demonstrate significant performance and cost advantages over the above-mentioned support materials. In short, LA/MFA/G (5 wt. %) is considered a promising candidate for use in low-temperature thermal energy storage.

Table 4. Comparison of the thermal properties of the prepared FSPCM with that of other materials in some of the literature.

Item	Melting Temperature (°C)	Solidifying Temperature (°C)	Latent Heat of Melting (J/g)	Latent Heat of Solidification (J/g)	References
Palmitic acid (25 wt. %)/active aluminum oxide	74.13	59.57	28.56	17.53	[51]
Capric–lauric acid (26 wt. %)/gypsum	19.11	—	35.24	—	[52]
Propyl palmitate(25–30 wt. %)/gypsun	19.0	16.0	40.0	—	[53,54]
Capric–palmitic acid (25 wt. %)/gypsum wallboard	21.12	21.46	36.23	38.28	[55]
Emerest 2326 (25.7 wt. %)/gypsum	16.32	19.7	34.77	33.97	[56]
Camphene–palmitic acid (55 wt. %)/FA	68.32	60.46	37.08	34.41	[57]
MA(13.11)/TiO ₂ –FA	52.22	26.68	23.43	22.57	[34]
Capric–myristic acid (20 wt. %)/vermiculite +EG (2 wt. %)	19.7	17.1	26.9	missing	[58]
LA(19.3 wt. %)/RFA	41.34	42.75	34.09	32.97	[33]
LA(44.8 wt. %)/CNT	35.02	missing	42.61	missing	[45]
LA/MFA/G(5 wt. %)	45.38	40.22	41.08	39.26	This study

3.5. Thermal Stability of the Prepared FSPCMs

The TGA curves of the LA, LA/MFA composite, and the LA/MFA/G (5 wt. %) FSPCM are illustrated in Figure 8. The degradation temperatures of the LA, LA/MFA composite, and the LA/MFA/G FSPCM occurred at 140 °C, 140 °C, and 160 °C, respectively, which were much higher than their working temperature of 40–47 °C. In addition, the weight losses of the LA/MFA composite and the LA/MFA/G (5 wt. %) FSPCM were about 26.88% and 22.49%, respectively, which were almost consistent with the adsorbed fraction of the LA into the MFA supporting matrix. The residual mass of the LA/MFA/G FSPCM was higher than that of the LA and LA/MFA FSPCM due to the lower encapsulation fraction of the LA.

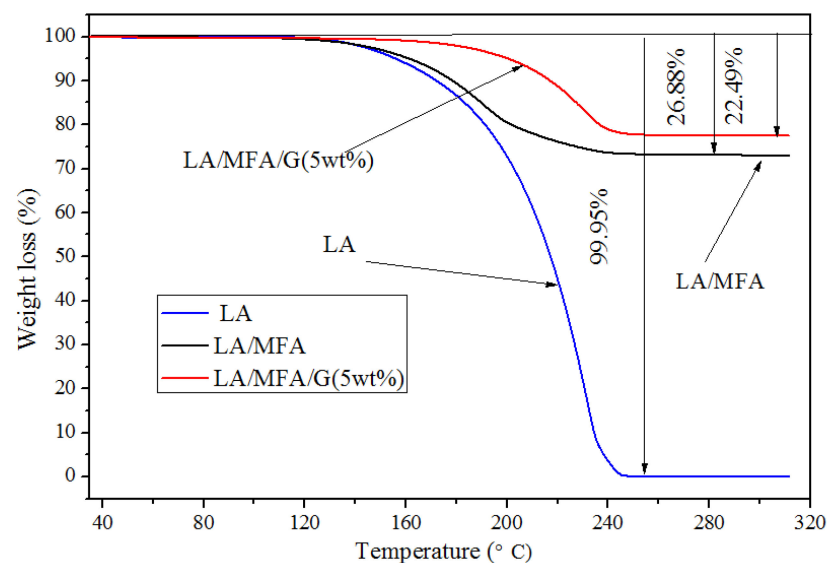


Figure 8. TGA curves of LA and LA/MFA and LA/MFA/G (5 wt. %).

Compared to LA, the fabricated LA/MFA/G (5 wt. %) FSPCM had a higher onset decomposition temperature, which demonstrated that MFA and G can make seepage-free FSPCMs more stable, owing to their high-temperature resistance characteristics. In other words, the thermal stability of LA/MFA/G FSPCM was enhanced by MFA and

G. These findings indicate that the LA/MFA/G FSPCM had excellent thermal stability within its working temperature, making it suitable for thermal energy storage in practical applications. Therefore, the LA/MFA/G FSPCM can be widely used in the low-temperature fields, especially in the field of building energy conservation.

3.6. Heat Transfer Efficiency of the Prepared FSPCMs

The heat storage/release performance curves of the synthesized composites were determined to evaluate their heat transfer efficiencies. As shown in Figure 9 and Table 5, it took about 18 min for the LA to undergo the melting process from 25 °C, while the LA/MFA composite and LA/MFA/G (5 wt. %) FSPCM took only about 15 min and 13 min, respectively. During the freezing process, it took about 36 min for LA to accomplish the freezing process to reach 25 °C, whereas the LA/MFA composite and LA/MFA/G (5 wt. %) FSPCM needed only about 17 min and 12 min, respectively. The heat transfer efficiency of the LA/MFA/G FSPCM was much higher than those of the LA and LA/MFA composites. Moreover, the time to maintain the equilibrium temperature of thermal energy storage in the melting process was about 9.5 min for the LA, about 5 min for the LA/MFA composite, and about 3.5 min for the LA/MFA/G (5 wt. %) FSPCM. In the freezing process, it took about 13 min for the LA, about 4.5 min for the LA/MFA composite, and about 2.5 min for the LA/MFA/G (5 wt. %) FSPCM to maintain the equilibrium temperature of thermal energy storage, which indicated that the thermal storage/release rate of the LA/MFA/G FSPCM was greatly enhanced with G as the thermal conductivity enhancer. In other words, the heat transfer efficiency of the LA/MFA/G FSPCM greatly improved. Compared with those of the LA, the thermal storage and release time of the LA/MFA/G (5 wt. %) FSPCM were decreased by 61.11% and 80.77%, respectively.

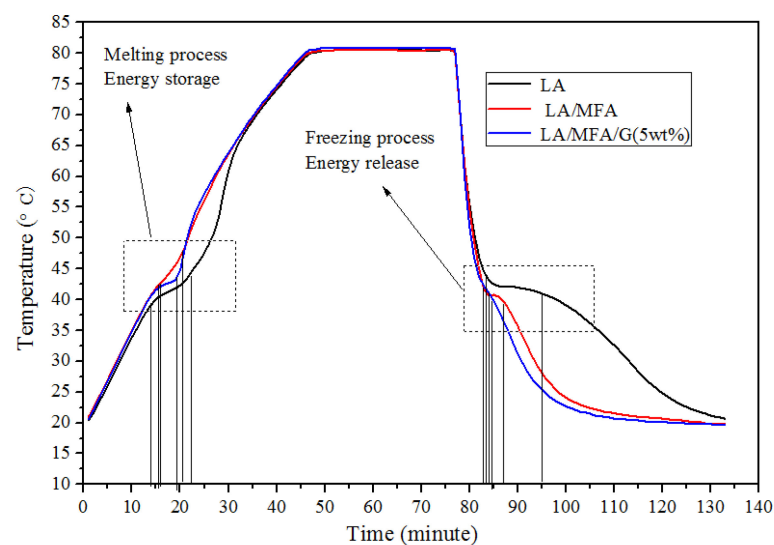


Figure 9. Storage and release curves of LA, LA/MFA, and LA/MFA/G (5 wt%).

Table 5. Comparisons of heat transfer times and rates among the prepared samples.

Sample	Heat Time (min)	Heat Storing Time (min)	Freezing Time (min)	Heat Releasing Time (min)	Improved Heat Rate (%)	Improved Freezing Rate (%)
LA	18	9	36	13	--	--
LA/MFA	15	5	17	4.5	44.44	65.38
LA/MFA/G (5 wt. %)	13	3.5	12	2.5	61.11	80.77

Through the above-mentioned comparison, it was clearly found that the MFA and G in the prepared composites shortened the melting and the freezing times, and indeed

improved the heat transfer rates during the melting and freezing processes. Practically, the introduction of G, together with MFA, significantly reduced the heat storing and releasing times, and improved the heat storing and releasing rates.

4. Conclusions

To provide a new utilization approach for FA and solve the leakage problem of PCMs, a low-cost and eco-friendly FSPCM was fabricated in this research, using LA as the PCM, MFA as the supporting matrix, and G as the thermal conductivity enhancer. A simple direct impregnation method with less experimental error was used. Firstly, the package efficiency and leakage resistance of MFA and G were evaluated. Using MFA with higher specific surface area and richer pore structure as a supporting matrix achieved a certain package efficiency and restricted the leakage of liquid LA. The introduction of G improved the loading capacity of MFA, which was consistent with the results of the SEM analysis; an impregnation ratio of 27.5% was achieved. Simultaneously, the LA/MFA (27.5 wt. %) /G (5 wt. %) had no leakage of LA and was considered to be the optimal FSPCM for its excellent performance in the chemical compatibility and thermal properties analyses. The LA/MFA/G had superior physical compatibility among the LA, MFA, and G. The phase change temperature of the LA/MFA/G (5 wt. %) was 45.38 °C for the melting process and 40.22 °C for the freezing process. Correspondingly, the enhanced thermal storage capacity with latent heat for melting and solidifying of the LA/MFA/G (5 wt. %) were determined as 41.08 J/g and 39.26 J/g, respectively. The results of the thermal stability tests for LA/MFA/G indicated that it had good thermal stability performance within its operating temperature. Meanwhile, the heat transfer efficiency of the LA/MFA/G (5 wt. %) FSPCM increased by 61.11% for the melting process and 80.77% for the freezing process. In summary, using MFA to pack LA via the direct impregnation method with a facile and less error-prone fabrication process resulted in good performance. Therefore, the LA/MFA/G FSPCM has the potential to be used for low-temperature thermal energy storage, such as in buildings. In conclusion, FA can be utilized to prepare FSPCMs that have great potential for the fabrication of new construction materials.

Author Contributions: Conceptualization, P.L. and Y.W.; methodology, P.L. and Y.W.; investigation, P.L. and J.R.; resources, J.R., Z.Z., X.C. and S.J.; writing—original draft preparation, P.L. and S.J.; writing—review and editing, P.L., Z.Z. and X.G.; supervision, Z.Z. and X.C.; project administration, X.C., Y.W. and X.G.; funding acquisition, Y.W. and X.G. All authors have read and agreed to the published version of the manuscript.

Funding: This research was jointly funded by the Key R&D Projects of Tibet Autonomous Region Science and Technology Program [XZ202101ZY0008G], the Science and Technology Project of Hebei Education Department [ZD2022053], the Fundamental Research Funds for the Universities in Hebei Province [QN2021142], Shenzhen Science and Technology Research Funding [No. JCYJ20190806165216555], and the Open Foundation of Hebei Key Laboratory of Green Development of Rock and Mineral Materials [RM202310]. And the APC was funded by [XZ202101ZY0008G] and [No. JCYJ20190806165216555].

Data Availability Statement: All data generated or analyzed during this study were included in this published article.

Conflicts of Interest: The authors declare no conflict of interest.

References

1. He, Y.; Li, X.; Huang, P.P.; Wang, J.N. Exploring the road toward environmental sustainability: Natural resources, renewable energy consumption, economic growth, and greenhouse gas emissions. *Sustainability* **2022**, *14*, 1579. [[CrossRef](#)]
2. Yong, Q.Q.; Tian, Y.P.; Qian, X.; Li, X.B. Retrofitting coal-fired power plants for grid energy storage by coupling with thermal energy storage. *Appl. Therm. Eng.* **2022**, *215*, 119048. [[CrossRef](#)]
3. Montes, M.J.; Linares, J.I.; Barbero, R.; Rovira, A. Proposal of a new design of source heat exchanger for the technical feasibility of solar thermal plants coupled to supercritical power cycles. *Sol. Energy* **2020**, *211*, 1027–1041. [[CrossRef](#)]
4. Tan, M.; Liu, W.D.; Shi, X.L.; Sun, Q.; Chen, Z.G. Minimization of the electrical contact resistance in thin-film thermoelectric device. *Appl. Phys. Rev.* **2023**, *10*, 021404. [[CrossRef](#)]

5. Khan, M.I.; Asfand, F.; Al-Ghamdi, S.G. Progress in research and technological advancements of commercial concentrated solar thermal power plants. *Sol. Energy* **2023**, *249*, 183–226. [[CrossRef](#)]
6. Ministry of Ecology and Environment of the People's Republic of China. *Annual Report on Prevention and Control of Solid Waste in China's Large and Medium-Sized Cities, 2020*; Environmental Protection in China: Beijing, China, 2020; p. 26.
7. Wang, C.; Xu, G.G.; Gu, X.Y.; Gao, Y.H.; Zhao, P. High value-added applications of coal fly ash in the form of porous materials: A review. *Ceram. Int.* **2021**, *47*, 22302–22315. [[CrossRef](#)]
8. Fernando, S.; Gunasekara, C.; Law, D.W.; Nasvi, M.C.M.; Setunge, S.; Dissanayake, R.; Robert, D. Environmental evaluation and economic analysis of fly ash-rice husk ash blended alkali-activated bricks. *Environ. Impact Assess. Rev.* **2022**, *95*, 106784. [[CrossRef](#)]
9. Yao, Z.T.; Ji, X.S.; Sarker, P.K.; Tang, J.H.; Ge, L.Q.; Xia, M.S.; Xi, Y.Q. A comprehensive review on the applications of coal fly ash. *Earth Sci. Rev.* **2015**, *141*, 105–121. [[CrossRef](#)]
10. Wang, C.Q.; Liu, K.; Huang, D.M.; Chen, Q.; Tu, M.J.; Wu, K.; Shui, Z.H. Utilization of fly ash as building material admixture: Basic properties and heavy metal leaching. *Case Stud. Constr. Mater.* **2022**, *17*, e01422. [[CrossRef](#)]
11. Geng, X.Z.; Duan, Y.F.; Zhao, S.L.; Hu, J.W.; Zhao, W.M. Mechanism study of mechanochemical bromination on fly ash mercury removal adsorbent. *Chemosphere* **2021**, *274*, 129637. [[CrossRef](#)]
12. Gao, K.; Iliuta, M.C. Trends and advances in the development of coal fly ash-based materials for application in hydrogen-rich gas production: A review. *J. Energy Chem.* **2022**, *73*, 485–512. [[CrossRef](#)]
13. Ghosh, D.; Ghose, J.; Datta, P.; Kumari, P.; Paul, S. Strategies for phase change material application in latent heat thermal energy storage enhancement: Status and prospect. *J. Energy Storage* **2022**, *53*, 105179. [[CrossRef](#)]
14. Panchal, J.M.; Modi, K.V.; Patel, V.J. Development in multiple-phase change materials cascaded low-grade thermal energy storage applications: A review. *Clean. Eng. Technol.* **2022**, *8*, 100465. [[CrossRef](#)]
15. Zhang, M.; Cheng, H.F.; Wang, C.Y.; Zhou, Y. Kaolinite nanotube-stearic acid composite as a form-stable phase change material for thermal energy storage. *Appl. Clay Sci.* **2021**, *201*, 105930. [[CrossRef](#)]
16. Alkhazaleh, A.H.; Almanaseer, W.; Alkhazali, A. Experimental investigation on thermal properties and fire performance of lauric acid/diphenyl phosphate/expanded perlite as a flame retardant phase change material for latent heat storage applications. *Sustain. Energy Technol.* **2023**, *56*, 103059. [[CrossRef](#)]
17. Wang, T.; Zhao, S.Y.; Liu, S.; Li, J.H.; Xin, Y.X.; Lu, Q.; Chen, H.J.; Liang, C. Effect of porous carbon on thermal and physical properties of composite pure alkane/expanded vermiculite phase change energy storage materials. *J. Energy Storage* **2022**, *54*, 105220. [[CrossRef](#)]
18. Ishak, S.; Mandal, S.; Lee, H.S.; Singh, J.K. Ph-controlled synthesis of sustainable lauric acid/SiO₂ phase change material for scalable thermal energy storage. *Sci. Rep.* **2021**, *11*, 15012. [[CrossRef](#)]
19. Wen, R.L.; Zhu, X.; Yang, C.; Sun, Z.H.; Zhang, L.Q.; Xu, Y.G.; Qiao, J.X.; Wu, X.W.; Min, X.; Huang, Z.H. A novel composite phase change material from lauric acid, nano-Cu and attapulgite: Preparation, characterization and thermal conductivity enhancement. *J. Energy Storage* **2022**, *46*, 103921–103927. [[CrossRef](#)]
20. Zhang, D.Y.; Li, C.C.; Lin, N.Z.; Xie, B.S.; Chen, J. Enhanced properties of mica-based composite phase change materials for thermal energy storage. *J. Energy Storage* **2021**, *42*, 103106. [[CrossRef](#)]
21. Liu, P.; Gu, X.B.; Bian, L.; Cheng, X.F.; Peng, L.H.; He, H.C. Thermal properties and enhanced thermal conductivity of capric acid/diatomite/carbon nanotube composites as form-stable phase change materials for thermal energy storage. *ACS Omega* **2019**, *4*, 2964–2972. [[CrossRef](#)]
22. Wu, S.F.; Yan, T.; Kuai, Z.H.; Pan, W.G. Thermal conductivity enhancement on phase change materials for thermal energy storage: A review. *Energy Storage Mater.* **2020**, *25*, 251–295. [[CrossRef](#)]
23. Mahnaz, F.; Fathallah, K.; Keyvan, R. Preparation of paraffin/silica-graphene shape-stabilized composite phase change materials for thermal energy storage. *J. Mater. Sci. Mater. Electron.* **2022**, *33*, 12846–12856.
24. Liu, Y.; Zheng, R.W.; Tian, T.; Li, J. Characteristics of thermal storage heat pipe charged with graphene nanoplatelets enhanced organic phase change material. *Energy Convers. Manag.* **2022**, *267*, 115902. [[CrossRef](#)]
25. Jin, W.Z.; Jiang, L.H.; Chen, L.; Yin, T.J.; Gu, Y.; Guo, M.Z.; Yan, X.C.; Ben, X.Q. Enhancement of thermal conductivity by graphene as additive in lauric-stearic acid/treated diatomite composite phase change materials for heat storage in building envelope. *Energy Build.* **2021**, *246*, 111087. [[CrossRef](#)]
26. Ren, M.; Zhao, H.; Gao, X.J. Effect of modified diatomite based shape-stabilized phase change materials on multiphysics characteristics of thermal storage mortar. *Energy* **2022**, *241*, 122823. [[CrossRef](#)]
27. Hong, Y.X.; Yan, W.T.; Du, J.; Li, W.Y.; Xu, T.; Ye, W.B. Thermal performances of stearic acid/sepiolite composite form-stable phase change materials with improved thermal conductivity for thermal energy storage. *J. Therm. Anal. Calorim.* **2021**, *143*, 3317–3329. [[CrossRef](#)]
28. Xie, N.; Gao, X.N.; Zhong, Y.; Ye, R.D.; Chen, S.; Ding, L.X.; Zhong, T.M. Enhanced thermal performance of Na₂HPO₄·12H₂O composite phase change material supported by sepiolite fiber for floor radiant heating system. *J. Build. Eng.* **2022**, *56*, 104747. [[CrossRef](#)]
29. Zhao, S.Y.; Li, J.H.; He, M.Y.; Song, S. Effects of Dopamine-Modified and Organic Intercalation on the Thermophysical Properties of Octadecane/Expanded Vermiculite Composite Phase Change Materials. *ACS Omega* **2022**, *7*, 13538–13545. [[CrossRef](#)]
30. Deng, Y. Effect of Ag nanowires on crystallization behavior of polyethylene glycol/expanded vermiculite composite phase change material. *J. Energy Storage* **2021**, *34*, 102223. [[CrossRef](#)]

31. Shi, J.B.; Li, M. Synthesis and characterization of polyethylene glycol/modified attapulgite form-stable composite phase change material for thermal energy storage. *Sol. Energy* **2020**, *205*, 62–73. [[CrossRef](#)]
32. Wen, R.L.; Xu, Y.F.; Xu, Y.G.; Sun, Z.H.; Zhang, L.P.; Qiao, J.X.; Wu, X.W.; Min, X.; Huang, Z.H. Attapulgite: A promising natural mineral as carrier material for fatty acids phase change material. *J. Therm. Anal. Calorim.* **2022**, *147*, 7203–7212. [[CrossRef](#)]
33. Xu, D.W.; Yang, H.M.; Ouyang, J.; Fu, L.J.; Chen, D.L. Lauric Acid Hybridizing Fly Ash Composite for Thermal Energy Storage. *Minerals* **2018**, *8*, 161. [[CrossRef](#)]
34. Genc, M.; Gen, Z.K. Microencapsulated myristic acid-fly ash with TiO₂ shell as a novel phase change material for building application. *J. Therm. Anal. Calorim.* **2018**, *131*, 2373–2380. [[CrossRef](#)]
35. Liu, P.; Gu, X.B.; Zhang, Z.K.; Rao, J.; Shi, J.P.; Wang, B.; Bian, L. Capric Acid Hybridizing Fly Ash and Carbon Nanotubes as a Novel Shape-Stabilized Phase Change Material for Thermal Energy Storage. *ACS Omega* **2019**, *4*, 14962–14969. [[CrossRef](#)]
36. Qiu, F.; Song, S.K.; Li, D.N.; Liu, Y.; Wang, Y.Q.; Dong, L.J. Experimental investigation on improvement of latent heat and thermal conductivity of shape-stable phase-change materials using modified fly ash. *J. Clean. Prod.* **2020**, *246*, 118952. [[CrossRef](#)]
37. Hekimoglu, G.; Nas, M.; Ouikhalfan, M.; Sari, A.; Kurbetci, S.; Tyagi, V.V.; Sharma, R.K.; Saleh, T.A. Thermal management performance and mechanical properties of a novel cementitious composite containing fly ash/lauric acid-myristic acid as form-stable phase change material. *Constr. Build. Mater.* **2021**, *274*, 122105. [[CrossRef](#)]
38. Arulselvan, S.P.; Gurusamy, S.V. Characterization of fly ash cenosphere-capric acid composite as phase change material for thermal energy storage in buildings. *Energy Sources Part A* **2022**, *44*, 2088–2102. [[CrossRef](#)]
39. Naresh, R.; Parameshwaran, R.; Ram, V.V.; Srinivas, P.V. Study on thermal energy storage properties of bio-based n-dodecanoic acid/fly ash as a novel shape-stabilized phase change material. *Case Stud. Therm. Eng.* **2022**, *30*, 101707. [[CrossRef](#)]
40. Liu, L.; Peng, B.; Yue, C.S.; Guo, M.; Zhang, M. Low-cost, shape-stabilized fly ash composite phase change material synthesized by using a facile process for building energy efficiency. *Mater. Chem. Phys.* **2019**, *222*, 87–95. [[CrossRef](#)]
41. Chen, Y.; Huang, Y.H.; Wu, M.; Wang, S. Fly ash/paraffin composite phase change material used to treat thermal and mechanical properties of expansive soil in cold regions. *J. Renew. Mater.* **2022**, *10*, 1153–1173. [[CrossRef](#)]
42. Gu, X.B.; Liu, P.; Peng, L.H.; Zhang, Z.K.; Bian, L.; Wang, B. Low cost, eco-friendly, modified fly ash-based shape-stabilized phase change material with enhanced thermal storage capacity and heat transfer efficiency for thermal energy storage. *Sol. Energy Mater. Sol. Cells* **2021**, *232*, 111343. [[CrossRef](#)]
43. Lv, P.Z.; Liu, C.Z.; Rao, Z.H. Experiment study on the thermal properties of paraffin/kaolin thermal energy storage form-stable phase change materials. *Appl. Energy* **2016**, *182*, 475–487. [[CrossRef](#)]
44. Ramakrishnan, S.; Wang, X.; Sanjayan, J.; Wilson, J. Assessing the feasibility of integrating form-stable phase change material composites with cementitious composites and prevention of PCM leakage. *Mater. Lett.* **2017**, *192*, 88–91. [[CrossRef](#)]
45. Feng, Y.H.; Wei, R.Z.; Huang, Z.; Zhang, X.X.; Wang, G. Thermal properties of lauric acid filled in carbon nanotubes as shape-stabilized phase change materials. *Phys. Chem. Chem. Phys.* **2018**, *20*, 7772–7780. [[CrossRef](#)]
46. Shen, Q.; Ouyang, J.; Zhang, Y.; Yang, H.M. Lauric acid/modified sepiolite composite as a form-stable phase change material for thermal energy storage. *Appl. Clay Sci.* **2017**, *146*, 14–22. [[CrossRef](#)]
47. Ma, F.K.; Liu, L.Q.; Ma, L.Q.; Zhang, Q.; Li, J.N.; Jing, M.; Tan, W.J. Enhanced thermal energy storage performance of hydrous salt phase change material via defective grapheme. *J. Energy Storage* **2022**, *48*, 104064. [[CrossRef](#)]
48. Jin, W.Z.; Jiang, L.H.; Chen, L.; Gu, Y.; Guo, M.Z.; Han, L.; Ben, X.Q.; Yuan, H.H.; Lin, Z.X. Preparation and characterization of capric-stearic acid/montmorillonite/graphene composite phase change material for thermal energy storage in buildings. *Constr. Build. Mater.* **2021**, *301*, 124102. [[CrossRef](#)]
49. Rao, Z.H.; Zhang, G.T.; Xu, T.T.; Hong, K. Experimental study on a novel form-stable phase change materials based on diatomite for solar energy storage. *Sol. Energy Mater. Sol. Cells* **2018**, *182*, 52–60. [[CrossRef](#)]
50. Ma, L.Y.; Wang, Q.W.; Li, L.P. Delignified wood/capric acid-palmitic acid mixture stable-form phase change material for thermal storage. *Sol. Energy Mater. Sol. Cells* **2019**, *194*, 215–221. [[CrossRef](#)]
51. Fang, G.; Li, H.; Cao, L.; Shan, F. Preparation and thermal properties of form-stable palmitic acid/active aluminum oxide composites as phase change materials for latent heat storage. *Mater. Chem. Phys.* **2012**, *137*, 558–564. [[CrossRef](#)]
52. Lv, S.L.; Zhu, N.; Feng, G.H. Eutectic mixtures of capric acid and lauric acid applied in building wallboards for heat energy storage. *Energy Build.* **2006**, *38*, 708–711.
53. Feldman, D.; Banu, D.; Hawes, D. Development and application of organic phase change mixtures in thermal storage gypsum wallboard. *Sol. Energy Mater. Sol. Cells* **1995**, *36*, 147–157. [[CrossRef](#)]
54. Karaman, S.; Karaipekli, A.; Sari, A.; Bicer, A. Polyethylene glycol (PEG)/diatomite composite as a novel form-stable phase change material for thermal energy storage. *Sol. Energy Mater. Sol. Cells* **2011**, *95*, 1647–1653. [[CrossRef](#)]
55. Sari, A.; Karaipekli, A.; Kaygusuz, K. Capric acid and myristic acid for latent heat thermal energy storage. *Energy Sources Part A* **2008**, *30*, 1498–1507. [[CrossRef](#)]
56. Feldman, D.; Banu, D. DSC analysis for the evaluation of an energy storing wallboard. *Thermochim. Acta* **1996**, *272*, 243–251. [[CrossRef](#)]

57. Genc, Z.K.; Canbay, C.A.; Acar, S.S.; Sekerci, M.; Genc, M. Preparation and thermal properties of heterogeneous composite phase change materials based on camphene-palmitic acid. *J. Therm. Anal. Calorim.* **2015**, *120*, 1679–1688. [[CrossRef](#)]
58. Karaipekli, A.; Sari, A. Capric–myristic acid/vermiculite composite as form-stable phase change material for thermal energy storage. *Sol. Energy* **2009**, *83*, 323–332. [[CrossRef](#)]

Disclaimer/Publisher’s Note: The statements, opinions and data contained in all publications are solely those of the individual author(s) and contributor(s) and not of MDPI and/or the editor(s). MDPI and/or the editor(s) disclaim responsibility for any injury to people or property resulting from any ideas, methods, instructions or products referred to in the content.